Proceedings of the 2014 ASME International Gas Turbine Institute
GT2014
June 16-20, Dusseldorf, Germany

GT2014-27329

A HYSTERESIS FOR A DS SUPERALLOY UNDER THERMOMECHANICAL FATIGUE

Thomas Bouchenot
University of Central Florida
Orlando, FL, USA

Ali P. Gordon
University of Central Florida
Orlando, FL, USA

Sachin Shinde
Siemens Energy
Orlando, FL, USA

Phillip Gravett
Siemens Energy
Orlando, FL, USA

ABSTRACT

Cyclic plasticity and creep are the primary design considerations of 1st and 2nd stage gas turbine blades. Directionally-solidified (DS) Ni-base materials have been developed to provide (1) greater creep ductility and (2) lower minimum creep rate in solidification direction compared to other directions. Tracking the evolution of deformation in DS structures necessitates a constitutive model having the functionality to capture rate-, temperature-, history-, and orientation-dependence. Historically, models rooted in microstructurally-based viscoplasticity simulate the response of long-crystal, dual-phase Ni-base superalloys with extraordinary fidelity; however, a macroscopic approach having reduced order is leveraged to simulate LCF, creep, and creep-fatigue responses with equally high accuracy. This study applies uncoupled creep and plasticity models to predict the TMF of a generic DS Ni-base, and an anisotropic yield theory accounts for transversely-isotropic strength. Due to the fully analytic determination of material constants from mechanical test data, the model can be readily tuned for materials in either peak- or base-loaded units. Application of the model via a parametric study reveals trends in the stabilized hysteresis response of under isothermal fatigue, creep-fatigue, thermomechanical fatigue, and conditions representative of in-service components. Though frequently considered in design and maintenance of turbine materials, non-isothermal fatigue has yet to be accurately predicted for a generalized set of loading conditions. The formulations presented in this study address this knowledge gap using extensions of traditional power law constitutive models.

1. INTRODUCTION

Modeling the thermomechanical fatigue (TMF) response of structures at the component level requires reduced order models that, rapidly converge. Materials such as Ni-base superalloys, steels, titanium alloys, etc. are routinely subjected to elevated temperature environments superimposed with mechanical loads where inelastic (e.g. plasticity and creep) strain energy is dissipated. A non-interactive (NI) modeling approach based on reduced order constitutive models has been developed to simulate the stabilized deformation response of a generic directionally-solidified (DS) Ni-base superalloy under TMF loading conditions. Such DS materials are approximated as transversely isotropic due to their elongated grains that are aligned with the primary stress axis of blades for turbomachinery. Suitable elastic, plastic, and creep models selected for the study have parameters that can be optimized analytically to regress data obtained with laboratory-tested specimens at temperatures and mechanical loads germane to component operating conditions. Tensile, low cycle fatigue (LCF), and creep deformation experiments conducted under isothermal conditions including, but not limited to, reference temperatures labeled as T1, T2, … , T9 were utilized for model correlation. These temperatures are labeled such that T1 < T2 < … < T9. Models were then utilized to predict stabilized hysteretic material responses under non-isothermal conditions. The NI model is demonstrated to simulate TMF data accurately under in-phase or out-phase loading with or without the presence of mean strain. Trends in the non-isothermal hysteresis response are compared with their isothermal counterparts. A newly-developed model presented here, based solely on isothermal constitutive modeling parameters, is shown to accurately predict the peak-valley stress response

under TMF conditions. This novel model has the capability to make first order approximations of TMF hysteresis and also life, when coupled with stress versus fatigue life prognostics approaches.

2. MATERIAL MODEL

The candidate material of this study is a generic directionally-solidified (DS), Ni-base superalloy, commonly applied as a first and second stage blading material in advanced land-based turbo-machines. Under service conditions, blades are bombarded with hot gas super-imposed with large centrifugal loads. Service-prompted attributes including quick starts, dwell periods, and rapid shut down facilitate localized hot/cold spots where thermomechanical fatigue cracks nucleate. Some DS materials that have been studied under TMF include: coated and bare [1] CM247LC DS, DS GTD-111 [2], DS René 80 [3], DS René 150, and various bare/coated specimens. A sketch of a typical microstructure of DS Ni-base superalloys is shown in Fig. 1. Here 0° corresponds to the longitudinal orientation (L-oriented), 90° is transversely-oriented (T-oriented), and the intermediate or bias orientation is selected at 45°. The area of grain boundaries (GBs) are minimized along the L orientation to add strength under creep and/or fatigue conditions.

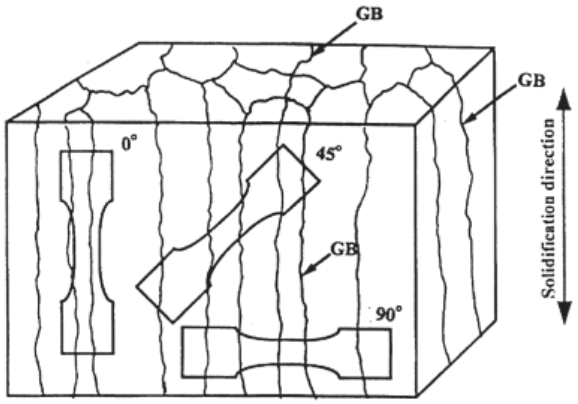

Figure 1: *Sketch of microstructure of a directionally-solidified (DS) Ni-base superalloy.*

In the course of predicting the stress-strain response of these materials, a variety of constitutive models have been invoked to capture the temperature-, rate-, and history-dependence of the non-linear kinematic and non-linear isotropic hardening that these materials display. Although continuum-level, viscoplasticity models [4] correlate well with test data, they have yet to usurp reduced order constitutive models native to general-purpose FEA full-scale component modeling. In the current study, the deformation response of select orientations (i.e., L, T, and 45, also referred to as bias) of a DS material is comprised of linear elastic, non-linear plastic (time-independent), and creep (time-dependent) components, i.e.,

$$\varepsilon_{total} = \varepsilon_{el}\left(\sigma,T,\theta\right) + \varepsilon_{pl}\left(\sigma,T,\theta\right) + \varepsilon_{cr}\left(\sigma,T,\theta\right) \quad (1)$$

Here T corresponds with temperature and the angle is referred to as θ. Each of these models capture orientation- and temperature-dependence; however, each is explicitly independent from the remaining deformation components. Decoupling creep from plastic deformation modes has the main advantage that LCF data can be used to analytically identify plasticity constant; similarly, steady-state creep data confers creep constants.

Elasticity modeling of the candidate DS material is carried out using Hooke's Law in three-dimensions. Based on symmetry, transversely isotropic materials can be described through five independent elastic constants: E_T, E_L, ν_{TT}, and ν_{TL}, G_{TL}. While the former four can be readily determined through uniaxial testing in L and T orientations, experiments in the bias (i.e., 45°-orientation) are used to analytically acquire the shear modulus.

Further, it should be noted that the elastic modulus for any direction within the LT-plane can be determined by means of

$$E\left(\theta\right) = \left[\frac{1}{E_L}\cos^4\theta + \left(\frac{4}{E_{45}} - \frac{1}{E_L} - \frac{1}{E_T}\right)\sin^2\theta\cos^2\theta + \frac{1}{E_T}\sin^4\theta\right]^{-1} \quad (2)$$

where, the angle θ is referenced from the DS (or L) orientation (Fig. 1). For most orthotropic materials, the peak elastic modulus of the material is located less than 10 degrees above from the bias orientation. The term G_{TT} corresponds to the shear modulus in the plane of isotropy. Each of these constants display temperature-dependence.

Time-independent plasticity modeling is implemented to do the following: (1) capture the strain hardening exhibited through the cyclic stress-strain DS material at various temperature levels, (2) capture the cyclic yield strength of the material, and (3) ensure that the material cannot support a stress above the cyclic ultimate tensile strength. Ramberg-Osgood plasticity is a two-parameter, power law model capable of satisfying each of these three requirements [5]. These parameters are the cyclic strain hardening coefficient, K', and the cyclic strain hardening exponent, n'. Typically, the Ramberg-Osgood model (and the associated Masing model used for reversals [6]) is used to interpolate the monotonic tensile response; however, for modeling the mid-life cyclic response of the material, the cyclic stress-strain curve of the material is utilized.

To capture the stress-saturation of the material extending beyond the cyclic proportional limit (CPL) of the material, the cyclic 0.2% offset yield strength (0.2%CYS) and the cyclic ultimate tensile strength (CUTS) are acquired. While the 0.2%CYS is defined in a similar manner to the monotonic 0.2% offset yield strength, CUTS is defined [7] to capture the scale up/down of the cyclic stress-strain curve compared to the monotonic analogy as reflected by the yield strengths. The ratio of the yield strengths extends the cyclic hardening or softening

trend out to the pseudo cyclic strength. Fig. 2 depicts the process of extrapolating low range LCF data into full range LCF data. The dashed line represents the case where LCF points are paired with monotonic yield and monotonic strength data. The dotted line illustrates LCF data alone.

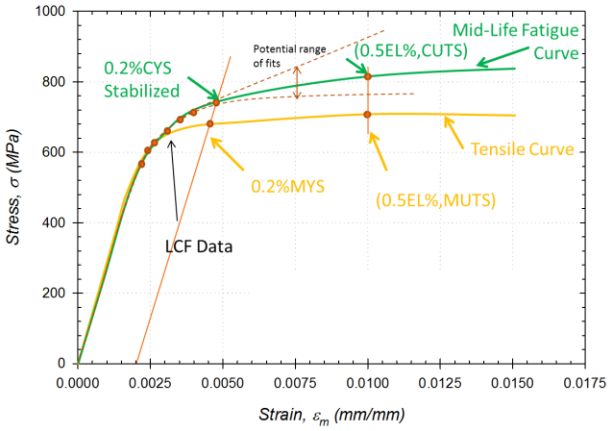

Figure 2: *Schematic of cyclic plasticity model determination.*

Since LCF data rarely exist beyond 0.2%CYS, this approach represents a viable method for modeling potentially large deformation responses. The solid line represents the optimal curve where LCF data are paired with cyclic yield and strength data. Beginning with the L-orientation of the material, the cyclic strain hardening constants, K' and n' are determined for each temperature.

Applied mechanics has produced a variety of failure theories for ductile materials. These yield theories vary based on capability to model levels of anisotropy, tensile-compressive asymmetry (i.e., sensitivity to hydrostatic stress), and so on [8]. With regard to DS materials in the current study, the Hill potential is employed due to its balance of simplicity, accuracy, and flexibility. Hill's theory states

$$\sigma_{Hill}=\left[\begin{array}{l}H\left(\sigma_x-\sigma_y\right)^2+F\left(\sigma_y-\sigma_z\right)^2+G\left(\sigma_z-\sigma_x\right)^2\\+2\left(L\tau_{yz}^2+M\tau_{zx}^2+N\tau_{xy}^2\right)\end{array}\right]^{\frac{1}{2}} \quad (3)$$

where F, G, H, L, M, and N are given as

$$\begin{aligned}F&=\frac{1}{2}\left(\frac{1}{R_{yy}^2}+\frac{1}{R_{zz}^2}-\frac{1}{R_{xx}^2}\right);\quad L=\frac{3}{2}\left(\frac{1}{R_{yz}^2}\right)\\G&=\frac{1}{2}\left(\frac{1}{R_{zz}^2}+\frac{1}{R_{xx}^2}-\frac{1}{R_{yy}^2}\right);\quad M=\frac{3}{2}\left(\frac{1}{R_{xz}^2}\right)\\H&=\frac{1}{2}\left(\frac{1}{R_{xx}^2}+\frac{1}{R_{yy}^2}-\frac{1}{R_{zz}^2}\right);\quad N=\frac{3}{2}\left(\frac{1}{R_{xy}^2}\right)\end{aligned} \quad (4)$$

where the R terms correspond to strength ratios between a given orientation and a reference orientation. For DS materials where the elongated grains are along the z-axis and the xy-plane is plane of isotropy,

$$\begin{aligned}R_{zz}&=R_{LL}=\frac{\sigma_L}{\sigma_0}=1\\R_{xx}&=R_{yy}=R_{TT}=\frac{\sigma_T}{\sigma_0}(T)\\R_{yz}&=R_{zx}=\sqrt{3}\frac{\tau_{yz}}{\sigma_0}=R_{LT,s}=\frac{\sigma_{45}}{\sigma_0}(T)\\R_{xy}&=\sqrt{3}\frac{\tau_{xy}}{\sigma_0}=R_{TT,s}=\frac{\sigma_T}{\sigma_0}(T)=R_{TT}\end{aligned} \quad (5)$$

Here, the reference orientation is defined as the L-orientation, and the reference strength, σ_0, is defined as the CUTS in the L-orientation. Although LCF data may be available in the T- and 45° orientations, only the CUTS or the 0.2%CYS points are obligatory. In this modeling approach, only the orientation-dependence of the strength is accounted for. Variations between the cyclic strain hardening between T and 45, compared to that of the L are neglected. Alternatively stated, in the plasticity relation that accounts for orientation-dependence, e.g.,

$$\varepsilon_{pl}=\left(\frac{\sigma_{Hill}}{K'}\right)^{\frac{1}{n'}} \quad (6)$$

only strength varies with orientation, while n' is isotropic.

Creep behavior of DS Ni-base materials is generally dominated by secondary and tertiary modes of deformation. Typically, tertiary creep strain is localized in turbine components, so modeling time-dependent deformation can be carried out with steady state creep models. Modeling the secondary creep response of a material can be executed using a number of second stage creep formulations. Most often, the Norton creep model is used to capture stress-dependence at a given temperature; however, the Garofalo model is able to capture the amplified creep rate of materials subjected to high stress levels [9], i.e.,

$$\dot{\varepsilon}_{cr}=A\left[\sinh\left(\alpha\sigma_{Hill}\right)\right]^n \quad (7)$$

where A, α, and n are regression constants that display temperature-dependence. Here the creep rate is taken as the minimum creep rate (or the slope during the secondary creep regime) for a given creep deformation and rupture curve. The Hill's potential serves the purpose of specifying the temperature-dependence and the shape of the yield surface in creep and plasticity [Eqs. (3)-(5)]. In the current study, only limited creep data are available (i.e., L- and T-orientations alone). Separate Hill's constants specific to creep and plasticity will be identified in future work. Considering that there are typically no available creep data above the yield strength of the

material, more points must be included to capture the stress-saturation behavior. A tensile strength anchor point is associated with a high strain rate, and it is considered as a conventional creep point.

3. DETERMINATION OF MATERIAL PARAMETERS

3.1 EXPERIMENTS AND MATERIAL DATA

Acquiring the mechanical properties required from the NI model formulation requires tensile, LCF, and creep deformation data. A variety of experiments of mechanics of materials was used to characterize the subject material of the study. In each case, test samples were cylindrically shaped, uncoated, and unnotched. Samples were machined from cast plates via low stress grinding and polishing of the gage section to eliminate machining marks, similar to a prior study by the authors [10]. Afterwards, data were analyzed and regressions constant were developed (Sec. 3.2).

Strain-controlled, tensile experiments were conducted on each orientation of the material at a range of temperatures. Experiments and consequent data conform to ASTM E8 [11]. A strain rate of $0.001s^{-1}$ ($6\%/min$) was used. Compared to specimens oriented either parallel or perpendicular to grains, fewer specimens were incised in the off-axis direction. Monotonic data were analyzed to for 0.2% yield strength (termed *0.2%MYS*) and monotonic ultimate tensile strength, *MUTS*.

Strain-controlled LCF testing was done on an MTS servo-hydraulic load frame. The identical strain rate employed for tensile testing was applied for the isothermal cyclic tests. A high temperature extensometer provided the strain measurement used for feedback control. Completely-reversed test conditions (i.e., $R_\varepsilon = -1$, $A_\varepsilon = \infty$) were employed, and tests were conducted to 50% drop of stabilized tensile load. Data was recorded at a minimum frequency of $1Hz$ as specified by ASTM E606 [10]. Strain amplitude levels were bracketed between 0.0010 and $0.015mm/mm$, depending on temperature and orientation. These experiments did not contain dwell periods.

Creep experiments were conducted on lever arm frames with dead weight loading. Tests were carried out until test samples completely ruptured. Stress levels were bracketed between 50 to $850MPa$, depending on temperature and orientation.

While tensile, LCF, and creep tests were used to validate the constitutive model formulation, non-isothermal fatigue data were gathered to verify the stabilized cyclic stress-strain model. Thermal cycling always followed the frequency of mechanical strain cycling with in- and out-of-phase conditions. A temperature rate of $5℃/sec$ was used in all cases. In some cases, mean strains were employed. Although a number of test specimens underwent post-test fractographic and microstructural analysis via white light optical microscopy (OM) and scanning electron microscopy (SEM), the discussion of observed damage mechanisms and how they relate to crack initiation life are reserved for future work.

3.2 PROCEDURE FOR PARAMETER IDENTIFICATION

Based on the experimental mechanics test program described in Sec. 3.1, an uncoupled elastic-plastic-creep deformation model was developed. Since the material model is designed to emphasize the stabilized hysteresis response of the DS Ni-base superalloy, measurements are derived via the mid-life response wherever possible. Analysis is focused on temperature levels of T1, T3, T4, T5, T6, T7, and T9 to capture temperature-dependence.

For the elastic response, high-order polynomial curve fits were used to interpolate the mid-life elastic response of the DS material in the L, T, and bias orientations. The most scatter in modulus occurs in the 45° orientation. Although the grains are elongated in the 45° (cf. Fig. 1), the number of grains that may appear in a cross-section can vary greatly. The orientation dependence of the mid-life modulus is shown for selected temperatures in Fig. 3.

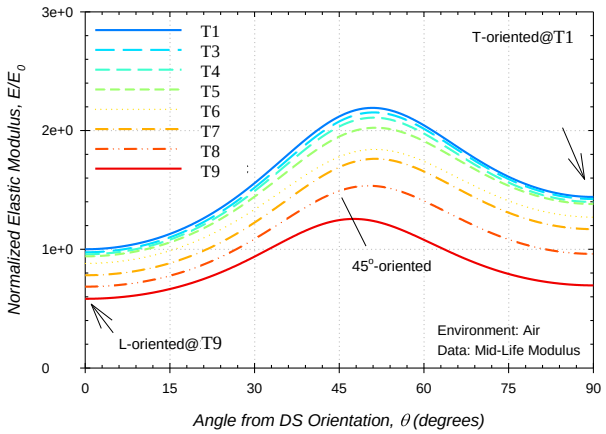

Figure 3: *Orientation- and temperature-dependence of a generic DS Ni-base superalloy.*

The peak modulus occurring at nearly at 52° is consistent with orthotropic materials where E_L is less than E_T. Weak temperature-dependence at low temperatures is illustrated by convergence of the curves, while strong temperature-dependence shows separation between curves. It should be noted that as temperature increases to T9, the central tendency of the curves begins to disappear. The material is generally less transversely-isotropic and increasingly more isotropic at high temperatures.

Beginning with the DS (or L) orientation, both K' and n' were determined by means of regressing Eq. (6) through stabilized stress-strain points. Typical data are shown in Fig. 4, and it should be noted that most LCF data emphasize the elastic region occurring at or beneath the CPL of the material. Properties from tensile curves were used to develop a pseudo stabilized cyclic UTS point. The monotonic and cyclic UTS points of the DS material are compared in Fig. 5. At low and

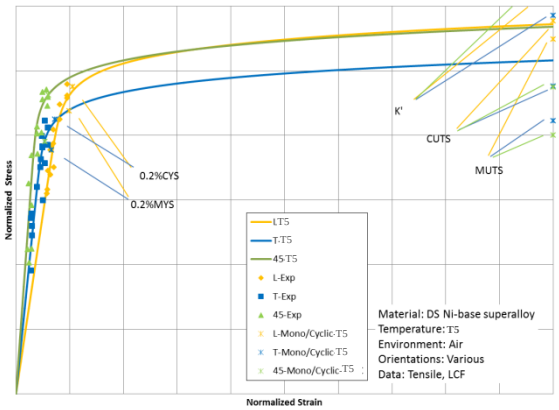

Figure 4: *Stabilized cyclic stress-strain response of select orientations of a generic DS Ni-base superalloy at a temperature of T5.*

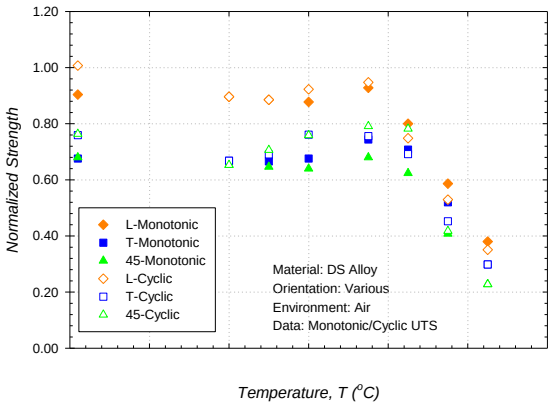

Figure 5: *Temperature-dependence of yield and tensile strength of select orientations of a generic DS Ni-base superalloy.*

moderate temperatures, the material is shown to cyclically harden, but this gives way to a softening response as temperature increases. Using this enhanced collection of points, K' and n' were determined for each temperature at which data were available (e.g. T1, T3, T4, T5, T6, T7, T8, and T9). The material model limits the DS material to cyclically work-harden at the same rate across the various orientations. The fit of the model through experimental LCF data for the transverse and bias orientations are optimized by manipulating the strength ratios given in Eq. (5).

Collecting the strength ratios between T (i.e., R_{TT}) and 45° (i.e., R_{LTs}) at the various selected temperatures must be carried out to fully develop the Hill's potential across the range of use of the material. Fig. 6 shows the normalized cyclic strength of the material along various orientations. Throughout the range of temperatures, the L orientation generally displays the maximum cyclic strength; however, as temperature increases the material exhibits isotropic strength under cyclic loading.

For each creep deformation curve, the minimum creep rate is determined. In some materials when the stress is in the range of and beyond the yield strength of the material, the strain rate

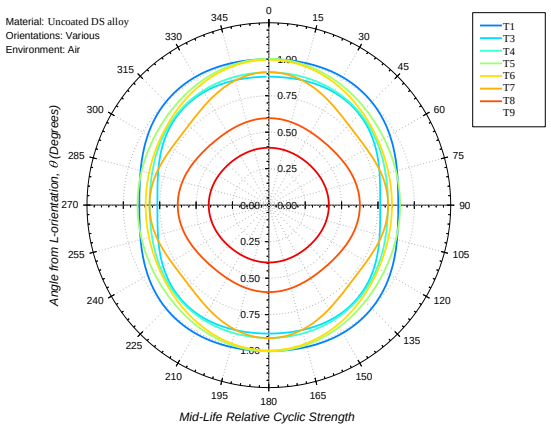

Figure 6: *Stabilized cyclic yield surface of a generic DS Ni-base superalloy at select temperatures.*

exhibited in materials may exceed that which is predicted by Norton creep. In the event that the stress level applied to the material escalates above the yield strength, the Garofalo model makes the creep rate of the material diverge.

For each temperature, stress versus creep rate data were regressed to optimize the fit of the Eq. (7). On the log-log scale, the trend with low stress creep data appears linear. Creep data are not available at either stress levels above the 0.2% yield strength or at key temperatures T1, T3, T4, T5, and T6. It should be noted that cast Ni-base superalloys have melting temperatures, T_m, in the range of 1300 to 1400°C. In most materials, creep deformation is negligible at and below $0.4T_m$. The modeling constants are considered are all temperature-independent and the Hill's parameters established earlier are carried over and applied to creep conditions.

3.3 RESULTS

The focus of this study on thermomechanical fatigue is that of a limited, but inclusive set of parametric simulations that replicate the diverse load histories and temperature profiles used in engineering practice. These include the maximum and minimum cycle temperature, the strain range, $\Delta\varepsilon$, strain ratio, phasing, and number of cycles. Factors such as the grain orientation, θ, and the addition of dwells are a focus of future research. To capture such a large set of loading conditions, a parametric study was conducted in ANSYS 14.0 Mechanical APDL using a single element model. APDL, short for ANSYS Parametric Design Language, is the FORTRAN-based programming equivalent to ANSYS Workbench, and allows simulations to be set up and conducted in a code-based environment. The parametric code performs displacement-controlled tests of a Solid185 element. Each side of the cubic, 8-node element has a length of $1mm$. A summary of the test parameters is shown in Table 1. The values of stress analyzed in this study are those associated with the component stress in the loading direction, though the material properties defined by the Garofalo creep model and the multilinear isotropic hardening model are directly modified by the Hill's anisotropy.

Table 1: *Summary of parametric testing parameters*

Condition, Symbol (Units)	Value
Strain Range, Δε (mm/mm)	0.0000 - 0.0125
LCF Test Temperatures, T (ref)	T2, T6, T7, T8
TMF Peak Temperatures, T_{max} (ref)	T6, T7, T8
TMF Valley Temperature, T_{min} (ref)	T2
TMF Phasing, φ	IP, OP
Strain Ratio, R (mm/mm)	0, -1, -∞
Hold Time, t_{hold} (hr)	0
Grain Orientation, θ (°)	90

LOW-CYCLE FATIGUE

Simulated completely-reversed LCF results (Fig. 7) at elevated strain ranges demonstrate a large inelastic deformation in the initial cycle, followed by a short period of strain-controlled hardening. Subsequent cycles are considered stabilized, with little change in plastic strain, though a decaying increase of magnitude in the maximum and minimum stress is observed. This causes the magnitude in peak and valley stresses to appear as a power law change over time. The hysteresis response includes tensile/compressive symmetry, which is an expected outcome of the material model.

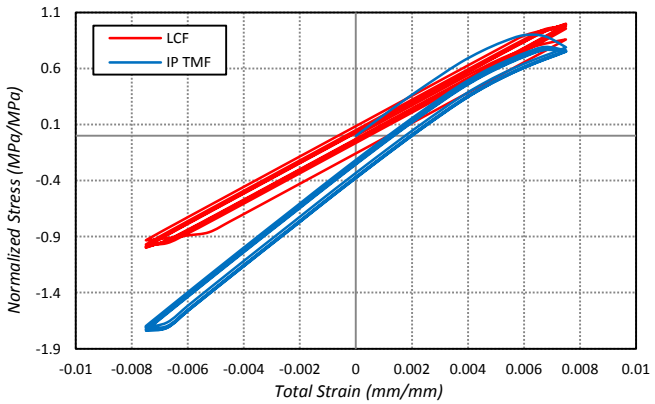

Figure 7: *Hysteresis plot of FEA results for an element subjected to a completely-reversed isothermal and IP non-isothermal load for three cycles at T8.*

LOW-CYCLE FATIGUE WITH MEAN STRESS

Hysteresis response for isothermal zero-to-tension and zero-to-compression loadings can be described as mirror images of one another resulting from the material symmetry; therefore, only the zero-to-tension case will be considered, which is shown in Fig. 8. Similar to the completely-reversed case, the plotted response contains a proportionally large quantity of inelastic strain in the first cycle. Subsequent cycles are predominantly elastic, with very little plasticity localized at the peak strain. The result is a straight line with a slight curvature at the end that creates a minor downward shift between cycles. The stress relaxation due to creep combined with strain hardening with continuous cycling lead to a mean stress that gradually reduces to zero.

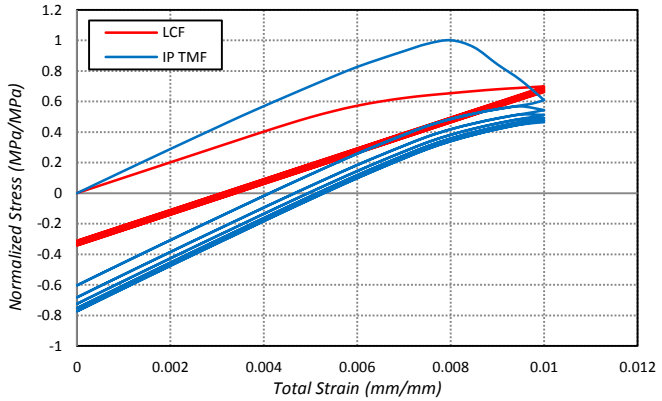

Figure 8: *Hysteresis plot of FEA results for an element subjected to a zero-to-tension isothermal and IP non-isothermal load for three cycles at T8.*

THERMOMECHANICAL FATIGUE

The IP and OP completely-reversed simulated hysteresis response takes the form of a traditional TMF loop, where the stress at the peak temperature contains a noticeable curvature and is lower in magnitude than the stress at the valley temperature. The completely-reversed IP and OP response is mirrored. The curvature and dissimilar stresses (Fig. 7) at the extremes are the result of the mechanical and thermal properties changing with respect to temperature. At T2, the elastic modulus and yield strength are larger than that of T8, but little to no creep is developed. The intermediate temperatures in the TMF cycle must also be considered. The dissimilarity of mechanical properties between temperatures, combined with the buildup of creep strain results in the curvature at the peak of each cycle, where the maximum stress is not necessarily at the maximum strain. As the number of cycle increases, the hysteresis loop is shifted downward by a decreasing amount.

Finite element analysis results are compared with experimental data of the first and mid-life cycle in Fig. 9. Although the material model is created from isothermal mid-life data, the simulated results exhibit a stronger resemblance to the first cycle TMF data. Closer examination reveals that the main source of error is derived from the response at the lower temperature. As the stress at this location is less than the yield strength of the material, no plastic deformation occurs in the simulation. In reality, changes in the yield surface and accumulated damage would allow this deformation to occur. It can be concluded that the plasticity model chosen for these simulations allows for a reasonable approximation, but a more complex, non-linear model is needed to increase fidelity.

TMF WITH MEAN STRESS

Due to the tensile/compressive symmetry of the material, only the zero-to-tension case is considered (Fig. 8). IP Results are similar to that of the completely-reversed case, though the effect of TMF on the shape of the hysteresis loop is more pronounced. Identical to the completely-reversed case, the first cycle experiences a large amount of inelastic deformation, which is stabilized in later cycles. This deformation has a

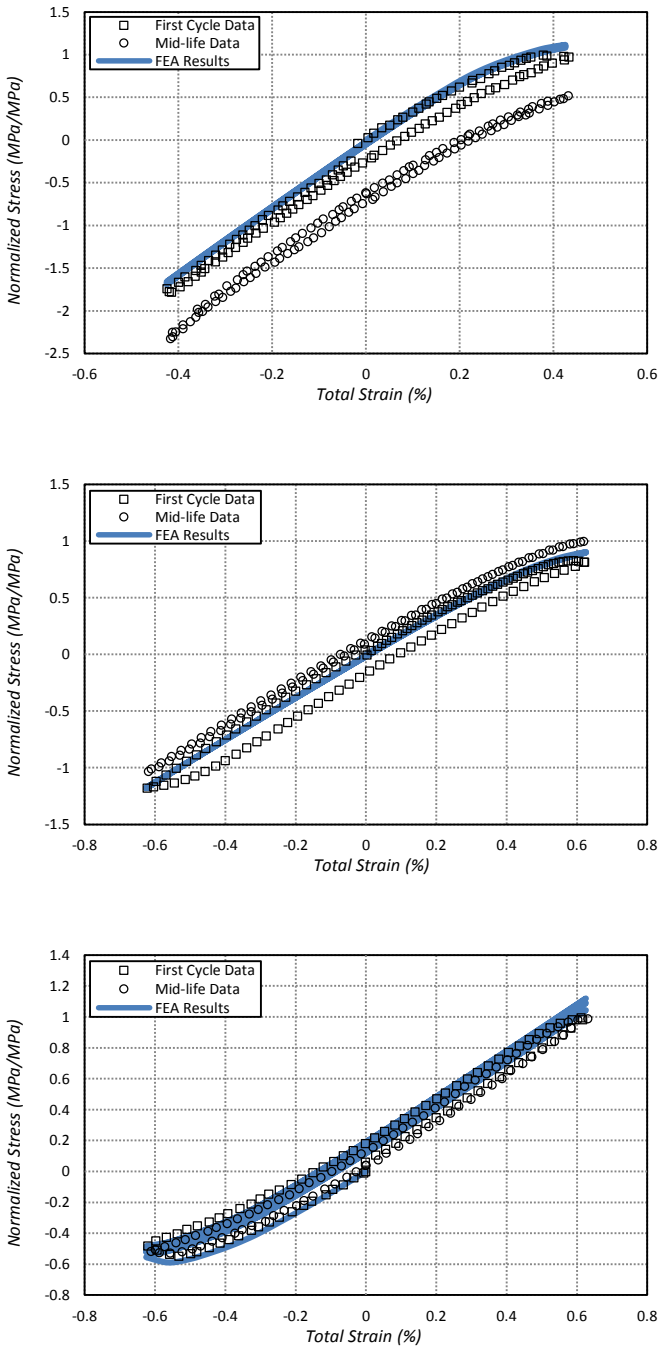

Figure 9: *FEA hysteresis data plotted against experimental results of a TMF completely-reversed (top) T2–T8 IP with a strain range of 0.0085 mm/mm (middle) T2-T7 IP with a strain range of 0.0125 mm/mm (bottom) T2-T8 OP with a strain range of 0.0125mm/mm.*

magnifying effect to the mismatch of peak stress and peak strain, where the stress appears to decrease in tension. After this initial cycle, the response at lower temperatures can be seen as a straight line that retraces its path after a minimum stress is reached, indicating that no plasticity or creep is developed in this stage. The response shifts downward with a decreasing amount in successive cycles. The OP loading condition is very similar to the isothermal condition at the minimum temperature. This is expected, as the maximum temperature associated with conditions that promote creep and plasticity, is coincident with the location of zero strain.

4. MODEL IMPROVEMENTS

Parametric test data in the following sections are presented in a unique plot where maximum and minimum stress is compared to their respective strain range. Individual graphs are created for each cycle number, maximum temperature and strain ratio. Each plot accounts for the isothermal response at the high temperature, isothermal response at the low temperature, IP TMF and OP TMF. The source of these plots is modeled in Fig. 10.

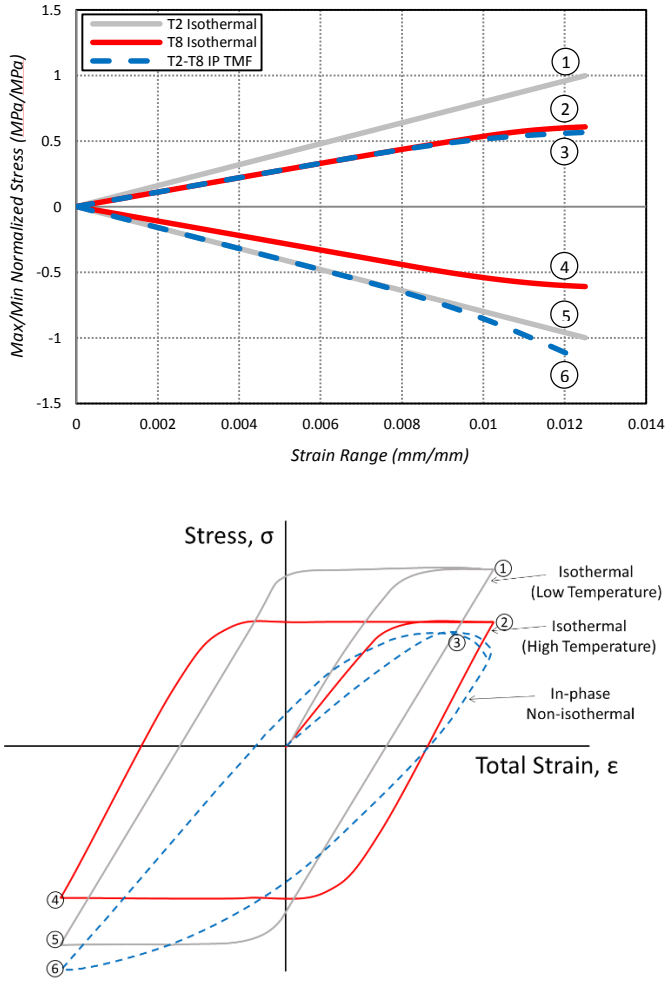

Figure 10: *(top) Sample minimum/maximum stress to strain range plot with (bottom) sketches of originating hysteresis loops.*

Each plot in this report contains normalized data after the response has stabilized. It should be noted that the LCF data used to correlate isothermal and non-isothermal response must be data acquired at the same rate and cycle number as the TMF test under consideration. Incorporation of a rate-dependent analysis method such as the Zener-Hollomon parameter, the Perzyna model, or the Peirce model [13] to conform to the standard testing rate of 0.001 mm/mm/s is a topic of future study.

The direct implementation of these relations into the findings of this study is a topic of future research. Though no concrete formulation has been presented, finite element results obtained in this study suggest that an equivalent relaxed stress obtained using a creep model at the maximum cycle temperature can be used to modify the cyclic hardening coefficient. This would provide a simple approximation of the rate-dependent effects in isothermal and non-isothermal stress prediction.

4.1 LOW-CYCLE FATIGUE

A constitutive model for estimating the minimum and maximum stress under thermomechanical fatigue using isothermal properties must begin with the analysis of LCF data. Incorporation of completely-reversed LCF data into the maximum/minimum stress to strain range (MSSR) plot are shown in Fig. 11. Due to the single element design and displacement-controlled test conditions, the resulting maximum and minimum stress occur at the maximum and minimum strain, respectively; therefore, the relation between strain range and maximum/minimum stress can be formulated using Ramberg-Osgood equation described in Sec. 2. However, for the completely-reversed case, a more accurate model can be achieved by employing a modification of the Masing's model traditionally established as

$$\Delta\varepsilon = \frac{\Delta\sigma}{E} + 2\left(\frac{\Delta\sigma}{2K'}\right)^{\frac{1}{n'}} \tag{8}$$

where $\Delta\varepsilon$ is the strain range and $\Delta\sigma$ is the stress range. Due to the tensile/compressive symmetric nature of the material, the maximum stress is equal to half the stress range, and the minimum stress is the negative of the maximum stress, resulting in

$$\Delta\varepsilon = \frac{2\sigma_{\max}}{E} + 2\left(\frac{2\sigma_{\max}}{2K'}\right)^{\frac{1}{n'}} \tag{9}$$

$$\sigma_{\min} = -\sigma_{\max}$$

where σ_{max} is the maximum stress and σ_{min} is the minimum stress. The result of this change on the MSSR plot is a reduction of the slope to half of the original value. A more accurate representation of the simulated data on a MSSR plot

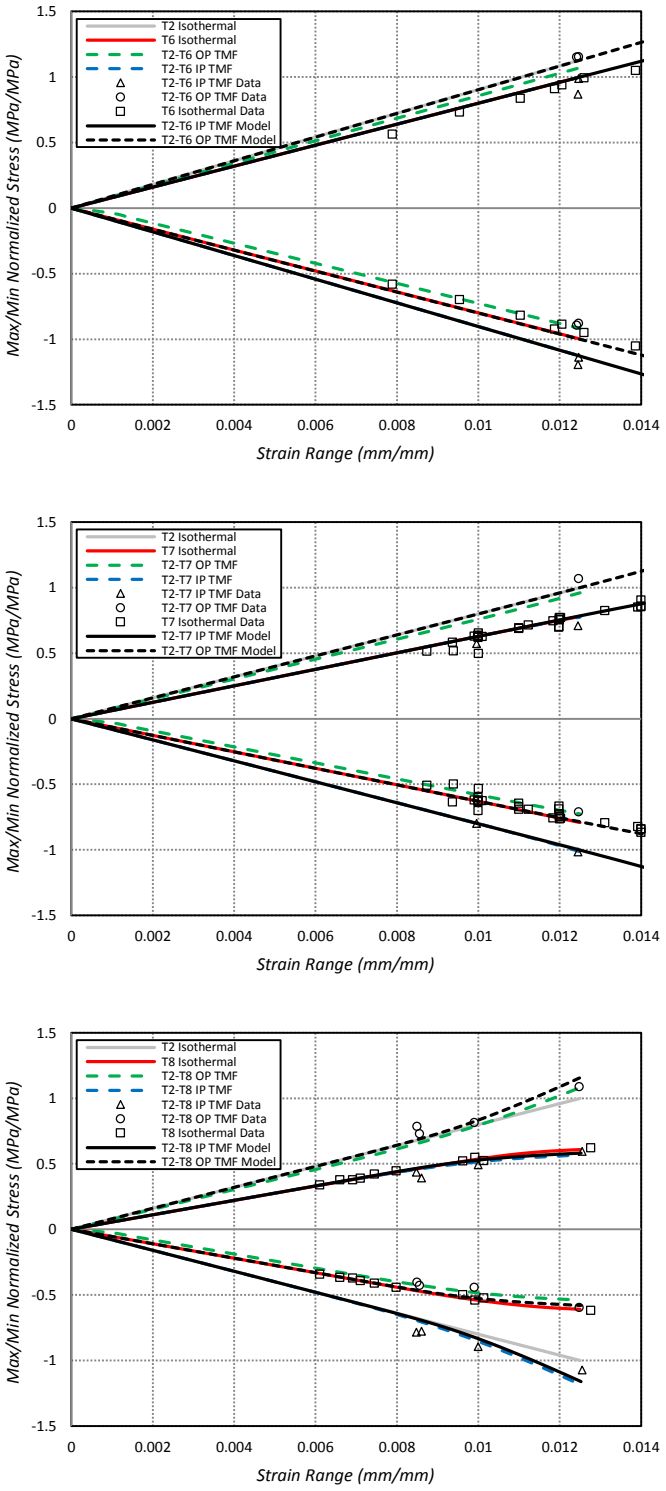

Figure 11: *MSSR plot of a (top) T2–T6, (middle) T2-T7, and (bottom) T2-T8 completely-reversed load with accompanying experimental data and formulated model.*

can be achieved by also using half the original value of the cyclic hardening exponent. This results in the expression

$$\Delta\varepsilon = \frac{2\sigma_{\max}}{E} + 2\left(\frac{2\sigma_{\max}}{2K'}\right)^{\frac{2}{n'}} \qquad (10)$$

$$\sigma_{\min} = -\sigma_{\max}$$

where the value of K' and n' are selected using LCF data at a TMF rate.

4.2 LOW-CYCLE FATIGUE WITH MEAN STRESS

Similar to the completely-reversed case, simulated zero-to-tension and zero-to-compression data can be analyzed on a MSSR plot, shown in Fig. 12, where a Ramberg-Osgood trend can be modeled for the maximum stress in zero-to-tension case. This relation is

$$\Delta\varepsilon = \frac{\sigma_{\max}}{E} + \left(\frac{\sigma_{\max}}{K'}\right)^{\frac{1}{n'}} \qquad (11)$$

In order to assess the effect of the mean stress, the minimum stress curve of zero-to-tension case is considered. The MSSR plot can be segmented into three distinct regions, outlined in Fig. 13. Strain ranges in which the maximum strain is unable to produce a stress that promotes yielding allows for purely elastic deformation (Region I). Therefore, the minimum stress is zero for this region. However, after plasticity is introduced (Region II), this minimum stress becomes negative, as the element is subjected to an elastic compressive stress at the minimum strain. Under extended strain range conditions, this minimum stress begins to deform plastically (Region III), which in turn affects the response at the maximum stress. A similar, though inverse, response can be seen for the zero-to-compression cases. In the following sections, the regions described above will be numbered according to the TMF response.

Analyzing the segment of the zero-to-tension plot that does not extend into Region III, we can conclude that the inelastic response at the maximum stress in Region I and II is the driving factor for the minimum stress. The minimum stress in Regions I and II is modeled as

$$\sigma_{\min} = -E\left(\frac{\sigma_{\max}}{K'}\right)^{\frac{1}{n'}} \qquad (12)$$

In Region III, where yielding occurs in the compressive region, the mean stress shifts to zero, even though the strain ratio indicates zero-to-tension loading. As the mean stress is zero, the minimum stress is equal to the negative maximum stress.

4.3 THERMOMECHANICAL FATIGUE

Superimposing isothermal and non-isothermal simulation data on a MSSR plot (Fig. 11) reveals that the shapes of both material responses are similar. Given a set of unknown E, K' and n' constants, an equation of similar form to Eq. (9) can be used to correlate the maximum and minimum stress to the strain range. The maximum stress of the IP loading is considered first.

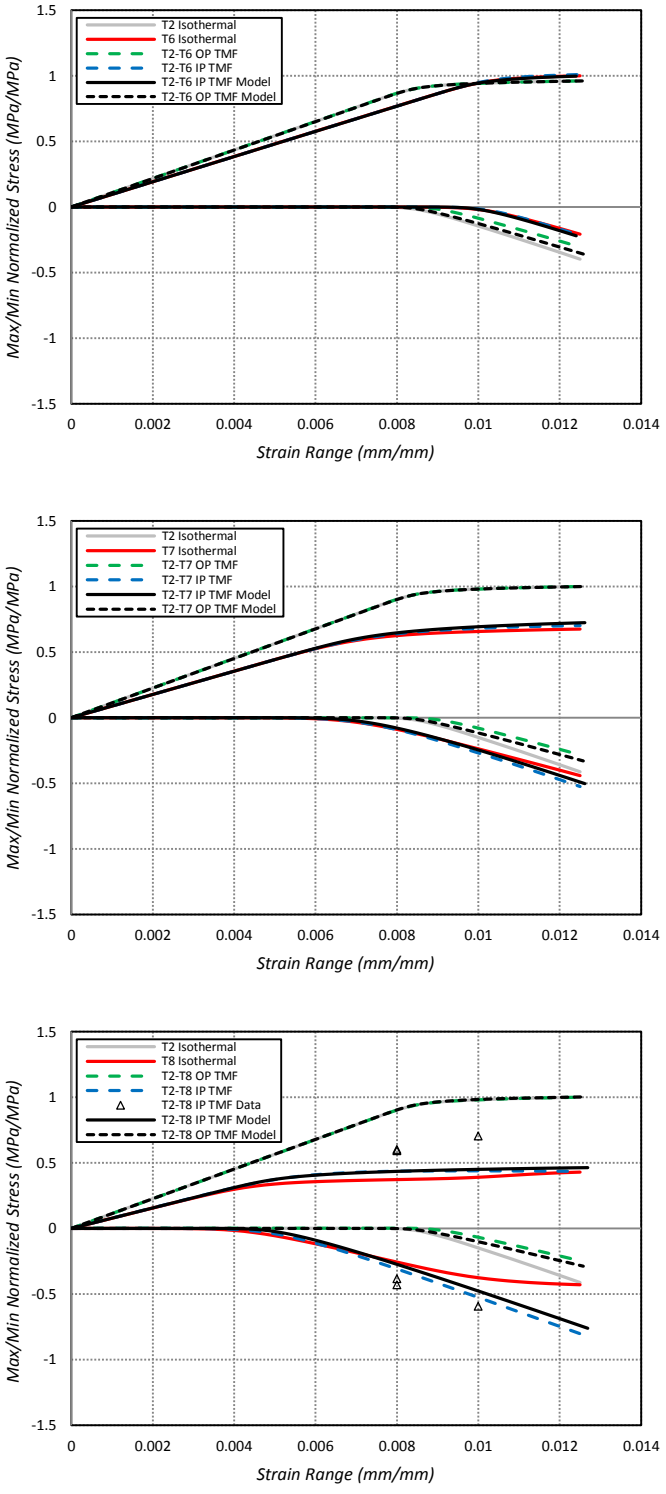

Figure 12: *MSSR plot of a (top) T2-T6, (middle) T2-T7, and (bottom) T2-T8 zero-to-tension load with formulated model.*

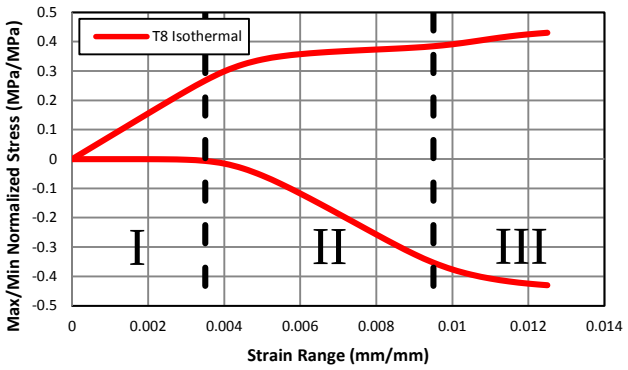

Figure 13: *Maximum/Minimum stress to strain range plot of simulated T8 isothermal data with separated regions.*

By inspection of Region I, the TMF equivalent elastic modulus of the maximum stress is equal to the elastic modulus at the peak temperature. Similarly, the equivalent elastic modulus of the minimum stress is equal to the elastic modulus at the lower temperature. In Region II, the resulting maximum and minimum stress of the TMF response are lower than that of the isothermal response. Simulated results show that the maximum stress can be successfully modeled using

$$\Delta\varepsilon = \frac{2\sigma_{\max}}{E_{iso,\max}} + 2\left(\frac{2\sigma_{\max}}{2K'_{iso,\max}}\right)^{\frac{1}{Bn'_{iso,\max}}} \tag{13}$$

where B is a unitless homologous modulus defined by

$$B = \frac{E_{iso,\max}}{E_{iso,\min}} \tag{14}$$

where $E_{iso,max}$ is the elastic modulus at the maximum temperature, $E_{iso,min}$ is the elastic modulus at the minimum temperature, $K'_{iso,max}$ is the cyclic hardening coefficient at the maximum temperature and $n'_{iso,max}$ is the cyclic hardening exponent at the maximum temperature. Effectively, the simple addition of a factor, B, into the Masing model allows for both isothermal and non-isothermal prediction of the maximum and minimum stress if the value of B is the homologous modulus in non-isothermal conditions, and 0.5 in isothermal conditions. In order to estimate the influence of creep, the isothermal elastic and plastic material properties used in these empirical correlations are those associated with a TMF strain rate.

In IP loading, the minimum stress response is strongly related to the isothermal response at the minimum temperature. As the material properties at the minimum temperature exhibit a yield strength higher than that of the maximum temperature, the minimum stress in the TMF response does not begin to yield at the same time as the maximum stress. That is to say, the curvature in the minimum stress response is only due to the plasticity and creep formed in the maximum stress. Therefore, in Region II, the minimum stress can be modeled as

$$\sigma_{\min} = -E_{iso,\min}\left(\Delta\varepsilon - \frac{\sigma_{\max}}{E_{iso,\max}}\right) \tag{15}$$

This model, as well as experimental data, is included in the MSSR plot of Fig. 11. Due to the symmetric nature of the material, an estimate of the OP response can be achieved by simply multiplying the resulting maximum and minimum stresses by a factor of -1.

4.4 TMF WITH MEAN STRESS

The MSSR plot for a zero-to-tension in-phase and out-of-phase response is shown in Fig. 12. Given the similarity with the zero-to-tension isothermal response, the maximum stress is expected to fit a Ramberg-Osgood relationship. The IP load condition is analyzed first.

The maximum stress in Region I contains the same slope as the isothermal response at the peak temperature. Therefore, the equivalent elastic modulus is the same value as that of the LCF at the peak temperature. The minimum stress in this region is zero, as the strain ratio indicates zero-to-tension, and no plasticity is developed. In Region II, the maximum stress under TMF is larger than the LCF case, which is unexpected, as the completely-reversed case results in a non-isothermal result that is lower than that of the isothermal response. The origin of these contrasting trends is a topic of future study, though the effect of creep is a likely factor. Despite this, the maximum stress in Region I and II can be formulated with Eq. (11) such that the values of K' and n' are those of isothermal data at the peak temperature at a non-isothermal strain rate, and the value of n' is multiplied by the homologous modulus. Similar to the completely-reversed case, the minimum stress can be related to the inelastic strain formed by the maximum stress. Therefore the minimum stress is approximated using Eq. (15). The non-isothermal response did not enter Region III in the strain range under consideration.

The maximum/minimum stress to strain range plot also reveals that the maximum stress in the OP case is nearly identical to that of the isothermal case at the minimum temperature. Therefore the maximum stress for an OP zero-to-tension load is calculated from Eq. (11) where the values of K' and n' are the cyclic hardening parameters evaluated at the minimum temperature. The value of minimum stress in the OP response is similar to that of the IP response, but is closely related to elastic modulus at the minimum temperature, formulated as

$$\sigma_{\min} = -E_{iso,\max}\left(\Delta\varepsilon - \frac{\sigma_{\max}}{E_{iso,\min}}\right) \tag{16}$$

In short, the maximum stress in an isothermal LCF or IP TMF zero-to-tension loading can be modeled using a modified Ramberg-Osgood model, where a homologous modulus is multiplied to the cyclic hardening exponent. In the OP TMF zero-to-tension loading, this homologous modulus is not needed, and is of the same form as the Ramberg-Osgood model.

5. CONCLUSIONS

Design of turbomachinery components subject to service conditions requires accurate approximations of hysteresis response. Under non-isothermal conditions, power-law plasticity models have been extended to predict peak/valley stress levels. Although the candidate material employed in the study is a DS Ni-base superalloy, it is plausible that the approaches developed here are applicable to cyclic stress-strain responses of two-parameter power law plasticity solids. The model was demonstrated to simplify if the temperature conditions become nominally isothermal. Ostensibly, the stresses in some components are thermally-driven, i.e., thermal fatigue. The novel model presented here is validated for zero-to-tension ($R_\varepsilon = 0$, $A_\varepsilon = 1$), and zero-to-compression ($R_\varepsilon = -\infty$, $A_\varepsilon = -1$) situations. Implementation of these approaches is realized as a set of parametric simulations exercised to provide non-isothermal results. Analysis of this data yields a collection of empirical models able to approximate the maximum and minimum stress under non-isothermal conditions. Though accurate, these formulations are straight-forward material-based extensions to the Ramberg-Osgood and Masing models.

ACKNOWLEDGMENTS

The authors are thankful for the constructive discussions concern FEA with Mr. Shahid Malik and Mr. Sankar Nelian. Mr. David Kosich and Mr. Tony Gringeri helped with experimental mechanics of materials.

REFERENCES

[1] Kowalewski, R., and Mughrabi, H., "Thermo-mechanical and isothermal fatigue of a coated columnar-grained directionally solidified nickel-base superalloy," ASTM Special Technical Publication 1371, *Symposium of Thermo-Mechanical Fatigue Behavior of Materials*, November 4th -5th, 1998.

[2] Gordon, A. P., Shenoy, M. M., and Neu, R. W., "A thermomechanical fatigue crack initiation model for directionally-solidified Ni-base superalloys," *11th International Conference on Fracture* 2005

[3] Abrokwah, E. O., Ojo, O.A., and Richards, N.L. "Failure mechanisms in thermomechanical fatigue of DS superalloy Rene 80," *Canadian Metallurgical Quarterly*, Vol. 51, No. 3, pp 356-66.

[4] Shi, D., Dong, C., and Yang, X., "Constitutive modeling and failure mechanisms of anisotropic tensile and creep behaviors of nickel-base directionally solidified superalloy," Materials & Design, Vol. 45, pp. 663-673, 2013.

[5] Masing G., "Eigenspannungen und Verfestigung beim Messing," *Proceedings of the 2nd international Congress of Applied Mechanics*, Zurich, 1926.

[6] Ramberg, W., and Osgood, W.R., "Description of stress-strain curves by three parameters. *Technical Note*, No. 902, National Advisory Committee for Aeronautics, Washington, D.C., 1943.

[7] Gordon, A. P., *Dictionary of Experiments of Mechanics of Materials*, Creative Printing and Publishing, Sanford, FL. 2012.

[8] Hill, R. "A theory of the yielding and plastic flow of anisotropic metals," *Proceedings of the Royal Society of London. Series A, Mathematical and Physical Sciences*, Vol. 193, No. 1033, pp. 281-297.

[9] Garofalo F., *Fundamentals of creep and creep rupture in metals*, New York: MacMillan, Inc., 1965.

[10] Shinde, S., and Gravett, P. "The Effects of Dwell on the LCF Behavior of IN617" *Journal of ASTM International*, Vol. 8, No. 8, 2011.

[11] ASTM, "Standard Test Method for Tension Testing of Metallic Materials (E08)," *ASTM Annual Book of Standards*, Vol., 03.01, 2013.

[12] ASTM, "Standard Test Method for Strain-Controlled Fatigue Testing (E606)," *ASTM Annual Book of Standards*, Vol., 03.01, 2012.

[13] Peirce, D., Shih, C.F., and Needleman, A., "A tangent modulus method for rate dependent solids," *Computers & Structures*, Vol. 18, pp.975-888, 1984.